# New Collector Undercut Technique Using a SiN Sidewall for Reduced $C_{bc}$ of InP/InGaAs SHBTs

*Kyungho Lee, Daekyu Yu, Minchul Chung, Jongchan Kang, Jeonghyeon Cha, and Bumman Kim*

**Dept. of E. E. Eng. and MARC, Pohang University of Science and Technology**

## Abstract

A new collector undercut process using SiN protection sidewall has been developed for high speed InP/InGaAs single Heterojunction Bipolar Transistors (HBTs). The HBTs fabricated using the technique have a larger base contact area, resulting in a smaller DC current gain and smaller base contact resistance than those of HBTs fabricated using normal undercut process. $C_{bc}$ is reduced to a comparable value for the two HBTs. Due to reduced base resistance, the maximum oscillation frequency ($f_{max}$) has been enhanced from 162 GHz to 208 GHz.

## 1. Introduction

Much effort has been made to reduce the base collector capacitance ($C_{bc}$) and base resistance ($R_b$) in HBT for a high speed operation since $f_{max} \cong (f_T/8\pi R_B C_{BC})^{1/2}$. Ion implantation technique is the most widely used for reduced $C_{bc}$ of GaAs HBTs but it is not a viable technique for InP-based HBTs [1]. Regrown base [2] and L-shaped base electrode [3] are used for reduction of $R_b$. Simple collector undercut is the most widely used to reduce the $C_{bc}$ of InP Double-HBTs due to the selective etching nature [4]. In the case of Single-HBTs, however, the base layer is also etched during the collector undercut process because selective etch cannot be employed.

In this paper, we propose a new collector undercut technique which does not etch the base layer laterally using SiN protection sidewall. Because the base contact layer is intact during the undercut, the contact resistance is maintained low. The RF performance data of the HBT clearly demonstrate the effectiveness of the new process technique.

## 2. Device Structure and Fabrication

The epitaxial layer of the fabricated HBTs is grown by Solid Source Molecular Beam Epitaxy (SSMBE) on a Fe-doped semi-insulating (100) InP substrate, starting with a 5000 Å InGaAs subcollector layer and 6000 Å thick, $2.0 \times 10^{16}$ cm$^{-3}$ Si-doped collector layer. The 600 Å InGaAs base is Be-doped to $3.0 \times 10^{19}$ cm$^{-3}$ with 70 Å spacer. The emitter layer is 1000 Å InP with Si-doped to $4.0 \times 10^{17}$ cm$^{-3}$.

Fabrication starts with the evaporation of Ti/Pt/Au emitter contact metals. Emitter etch was carried out by two selective wet processes, and was slightly undercut. After the emitter etch, a self-aligned Pt/Ti/Pt/Au base metal was evaporated [Fig. 1 (a)]. The emitter was protected by photo-resist using base contact mask and the base and collector layers were then etched. Next, Polyimide was coated, and then flatly etched without mask using $O_2$ RIE until the emitter metal was exposed. Next, a Ti/Au emitter widening metal was evaporated [Fig. 1 (b)], and second polyimide etch was performed until the thickness of the residual polyimide is about 2000 Å. Next, SiN was deposited [Fig. 1 (c)]. The SiN was mask etched and the residual polyimide was removed by ashering [Fig. 1 (d)]. The collector was undercut but the base layer was protected by the SiN sidewall. The subcollector was etched for isolation, and AuGe/Ni/Au collector ohmic metal and pad metal were evaporated and alloyed. Au air-bridge formation followed. For comparison, normally processed HBTs were also built. We call the former HBT-N and the latter HBT-C. The schematic cross sections of both devices used for evaluations are shown in Fig. 2 (a) and (b).

## 3. Results and Discussion

The I-V curves of the two HBTs with $1 \times 20$ μm$^2$ emitter area were measured and depicted in Fig. 3. As shown, the common-emitter dc current gain ($\beta$) of the HBTs are about 23 and 14 for HBT-C and HBT-N, respectively, at a collector current density of $1 \times 10^5$ A/cm$^2$. In order to explain the difference of DC current gains of the devices, the base currents were decomposed using the following relationship,

$$J_C \frac{1}{\beta} = J_{BA} + 2J_{BP}\left(\frac{1}{W_E} + \frac{1}{L_E}\right) \quad (1)$$

where $J_{BA}$ is the base current component which is proportional to the emitter area, $J_{BP}$ is the base current component which is proportional to the emitter periphery. We found $J_{BA}$ of 15.72 μA/μm$^2$ and 15.83 μA/ μm$^2$ and $J_{BP}$ of 6.11 μA/μm and 11.77 μA/μm at a collector current density of $5 \times 10^4$ A/cm$^2$ for HBT-C and HBT-N, respectively. Since both devices were made with the same wafer and the same process, except the collector undercut step, the two devices are identical except the undercut area. As shown in Fig. 2, HBT-N has a large base contact area compared to HBT-C. Therefore, it has a larger contact recombination current and has a lower $\beta$.

Fig. 4 and 5 show RF characteristics of the HBT-C with HBT-N. The $f_T$ and $f_{max}$ of HBT-C are 78 GHz and 162 GHz, respectively, at $I_C$=14.3 mA and $V_{CE}$=2.0 V, and those of HBT-N are 80 GHz and 208 GHz, respectively at the same bias point. These differences can be attributed to the differences in base resistance $R_b$, since $f_{max}$ is dependent on $R_b$. Therefore, we have investigated $R_b$, which is given by

$$R_b = \frac{R_{SB}S_E}{12L_E} + \frac{R_{SB}S_{EB}}{2L_E} + \frac{\sqrt{\rho_{BC}R_{SB}}}{2L_B}\coth S_B\sqrt{\frac{R_{SB}}{\rho_{BC}}} \quad (2)$$

where $R_{SB}$ is base sheet resistance, $S_E$ and $S_B$ are emitter and base widths (1.0 μm in our case), $L_E$ and $L_B$ are emitter and base lengths, respectively, $S_{EB}$ is emitter to base spacing (0.2 μm), and $\rho_{BC}$ is base specific contact resistivity. Base sheet resistance of 640 Ω/□ and specific contact resistivity of $3.0 \times 10^{-6}$ Ω•cm$^2$ were measured using TLM. The transfer length, $L_T$, expressed as $(\rho_{BC}/R_{SB})^{1/2}$ is 0.68 μm. As shown in Fig. 2 (b), the effective base contact width becomes narrower for HBT-C due to the lateral etch of the base layer. $R_b$ of the device can be increased exponentially as the base contact area becomes narrower than $L_T$ (see the last term of Eqn. (2)). Thus, $R_b$ of the HBT-C can be large. Since the base contact layer of HBT-N is maintained intact during the collector undercut

formation, it is expected that the $R_b$ of HBT-N will be lower.

To estimate the total base resistance $R_b$, the small signal model parameters of the two HBTs were extracted and listed in Table I. As shown, both devices have similar values of $C_{bc}$, indicating that the capacitances are reduced successfully for both devices. However, the base resistances are quite different, 31.5 Ω and 20.4 Ω for HBT-C and HBT-N, respectively. This data clearly shows that the new process with SiN protection wall is working properly. Consequently, $R_b$ is reduced by 35% and maximum oscillation frequency, $f_{max}$, is enhanced by 30%. Since $R_b$ does not affect the transit time, $f_T$'s of the two HBTs are quite similar, around 80 GHz.

| | $R_E$ (Ω) | $R_B$ (Ω) | $g_m$ (mS) | $r_\pi$ (Ω) | $C_\pi$ (pF) | $C_{bci}$ (fF) | $C_{bcx}$ (fF) |
|---|---|---|---|---|---|---|---|
| HBT-C | 1.38 | 31.5 | 552 | 48.3 | 1.14 | 3.15 | 10.82 |
| HBT-N | 1.42 | 20.4 | 544 | 40.1 | 1.05 | 3.04 | 10.94 |

Table I. Extracted small-signal parameter of the fabricated HBT with $1\times20\mu m^2$ emitter area.

## 4. Conclusions

In order to reduce $C_{bc}$ without increasing $R_b$, we have developed a new collector undercut process using a SiN protection sidewall. Since the base layer is intact during the collector undercut formation, it maintained a wide base contact region, while the region for conventional process is laterally etched. Due to the wide base contact region, the HBTs have a smaller current gain and smaller base resistance with similar $C_{bc}$ compared to the HBTs with conventional process. We have demonstrated a 35% reduction of base resistance and a 30% increase of $f_{max}$. $f_{max}$ is enhanced from 162 GHz to 208 GHz for $1 \times 20\ \mu m^2$ emitter HBTs.

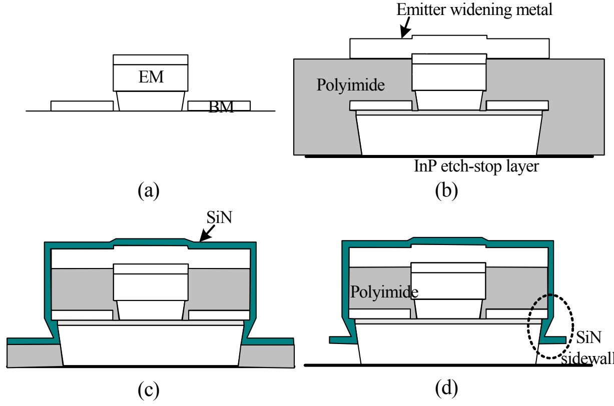


Fig. 1. Process flow of new collector undercut technique. (a) Self-aligned base metal, (b) Emitter metal widening, (c) SiN deposition, (d) Removal of residual polyimide.

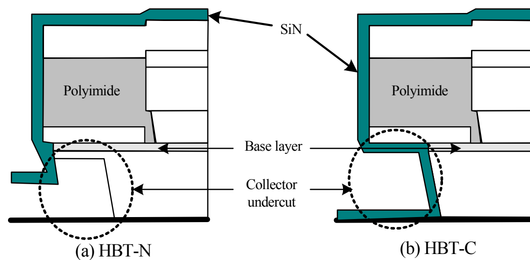


Fig. 2. Schematic cross sections of fabricated devices: (a) HBT-N with new undercut process and (b) HBT-C with conventional undercut process.

## 5. References


[1] M.-C. Ho, et al., "High-Performance Low-Base-Collector Capacitance AlGaAs/GaAs HBTs Fabricated by Deep Ion Implantation," *IEEE Electron Device Letters*, vol. 16, no. 11, pp. 512-514, 1995.

[2] Hidenori Shimawaki, et al, "High-fmax AlGaAs/InGaAs and AlGaAs/GaAs HBT's with p+/p Regrown Base Contacts," *IEEE Trans. Electron Devices*, vol. 42, no. 10, pp. 1735-1744, 1995.

[3] Manabu Yanagihara, et al, "253-GHz $f_{max}$ AlGaAs/GaAs HBT with Ni/Ti/Pt/Ti/Pt-Contact and L-Shaped Base Electrode," *Tech. Dig. IEEE IEDM*, 1990, pp. 807-810.

[4] I. Schnyder, M. et al, "A Laterally Etched Collector InP/InGaAs(P) DHBT Process for High Speed Power Applications," *Proc. Int. Conf. IPRM*, pp. 477-480, 2000.


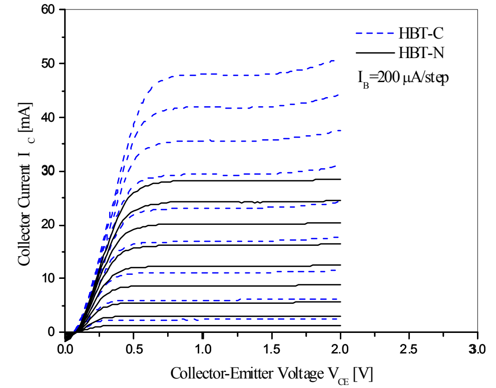


Fig. 3. Common emitter $I_C$-$V_{CE}$ characteristics of HBT-C and HBT-N

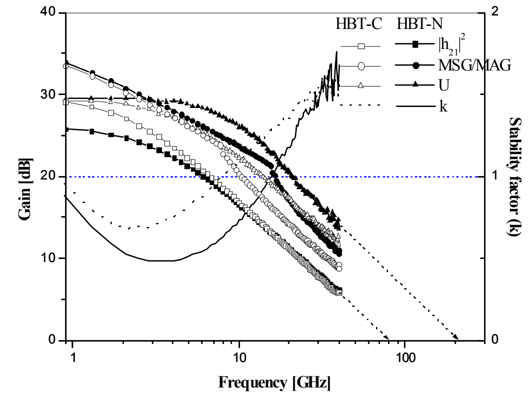


Fig. 4. Frequency dependencies of $|h_{21}|^2$, MSG/MAG, U, and stability factor(k) as determined by S-parameter measurements.

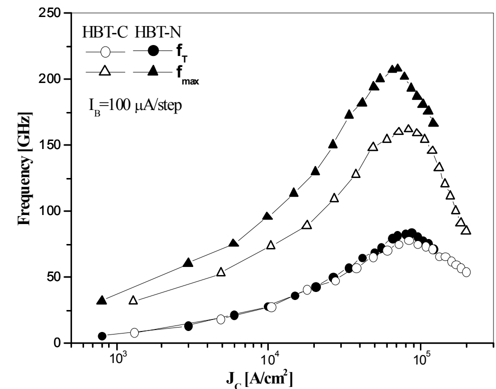


Fig. 5. Dependence of $f_T$ and $f_{max}$ on collector current density for HBT-C and HBT-N at $V_{CE}$=2.0 V.